Practical application of global siliciclastic rock-property trends to AVA interpretation in frontier basins

David J. Went[1]

https://doi.org/10.1190/tle40060454.1

Abstract

Global empirical relationships of P-wave to S-wave and density for sandstones and shales are used to model two-term amplitude variation with angle at various depths of burial in a typically compacting siliciclastic basin. Data from the normally pressured Tertiary strata of Judd Basin, Atlantic Margin, West of Shetland, are used as a control. For a typical prospect depth of 1750 m below mudline, forward models of angle-dependent reflectivity reveal that discrimination of lithology (shale and brine sand) and fluid (oil sand) is optimally resolved at a 47° incidence angle (θ). This is equivalent to an angle of 28° on an intercept-gradient crossplot. Repeat experiments at other depths produce similar results but with the angle for optimal lithology and fluid determination shifting slightly with increasing depth. Background trends in seismic data crossplots of intercept versus gradient are typically overprinted by noise that has a disproportionate effect on the gradient. This study suggests that the difference between the noise and background rock-property trend is relatively small, such that in most modern seismic data sets, anomalies should be identifiable on time-windowed crossplots and equivalent weighted stacks. It is proposed that a seismic inversion for relative extended elastic impedance at a 45° incidence angle should capture most anomalies of interest in frontier basins with simple burial histories. An example is illustrated from a seismic line in Mozambique.

Introduction

Typically, global frontier exploration is conducted with seismic data and little or no well control. The explorationist is looking to establish play fairways and develop leads for further analysis. Stack seismic data are generally good for determining the structure of the subsurface but are less well suited to the identification of lithology and fluid type. Prestack seismic inversion has the potential to identify lithology and fluid content through amplitude variation with angle (AVA) analysis. The purpose of this paper is to show the results of an experiment that demonstrates how global empirical relationships of P-wave to S-wave and density for sandstones and shales can be used to help predict AVA behavior when exploring frontier basins with simple burial histories (e.g., passive margins). The physical and seismic properties of sandstones and mudstones are reviewed, and established empirical relationships are used to build forward models of angle-dependent reflectivity. This exercise reveals that in simply buried siliciclastic systems, lithology and fluid typically can be resolved at most depths of interest by using a two-term extended elastic attribute at a 45° incidence angle. A simple intuitive seismic inversion routine is outlined and applied to a seismic line in Mozambique to show how screening for AVA anomalies may be performed by interpreters during the exploration process.

Rock properties and angle-dependent reflectivity — The Shuey equation

The contrasting properties of sedimentary rocks at a reflecting interface determine angle-dependent reflectivity (Figure 1). For incidence angles of 0°–35°, this is most simply described in terms of intercept and gradient by using Shuey's two-term approximation to the Zoeppritz equation (Shuey, 1985; Avseth et al., 2005). Three variables enable us to create a forward model of seismic reflectivity: P-wave velocity (V_P), S-wave velocity (V_S), and density (ρ). Two rock properties derived from these variables, acoustic impedance (AI) (ρV_P) and V_P/V_S, are critical for understanding the seismic response. The first term in Shuey's equation, A, is the AVA intercept. It defines the seismic reflectivity at zero offset and is defined by contrasts in AI across the interface. The second term in Shuey's equation, B, is the AVA gradient, or the rate at which reflectivity increases or decreases with angle. It is defined by changes in V_P, V_S, V_P/V_S, and ρ (equation 1). In most

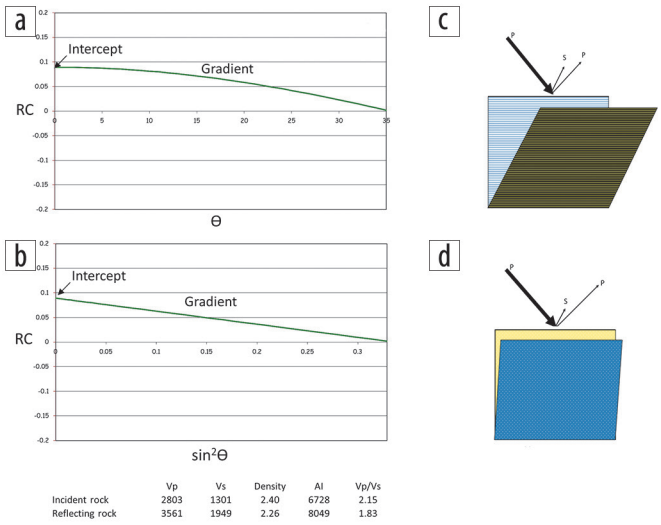

Figure 1. (a) Forward model of angle-dependent reflectivity for the specified velocity and density data using Shuey's two-term equation: $RC = A + B\sin^2\theta$, where $A = 0.89$ and $B = -0.266$. (b) Plotting the incidence angle as $\sin^2\theta$ linearizes the reflectivity model and facilitates measurement of the gradient. (c) The incident rock in this example is more susceptible to shear than (d) the reflecting rock.

[1]TGS ASA, Woking, UK. E-mail: david.went@tgs.com.

instances, the contrast in V_P/V_S is the dominant control on the AVA gradient. The gradient is measured on an axis of $\sin^2\theta$. A good approximation to reflectivity, which is valid for a 0°–35° incidence angle, is given by $A + B \sin^2\theta$ (Shuey, 1985).

$$\text{Intercept } A = \frac{1}{2}\left(\frac{\Delta V_P}{\overline{V_P}} + \frac{\Delta\rho}{\overline{\rho}}\right)$$

$$\text{Gradient } B = \frac{1}{2}\frac{\Delta V_P}{\overline{V_P}} - 2\frac{\overline{V_S}^2}{\overline{V_P}^2}\left(\frac{\Delta\rho}{\overline{\rho}} + 2\frac{\Delta V_S}{\overline{V_S}}\right). \quad (1)$$

The V_P, V_S, and ρ of sandstones and shales are commonly measured in boreholes, primarily in the form of sonic and density logs. These data, collected from basins around the world, have enabled the relationships between lithology and acoustic properties to be established so they can be used to understand seismic responses when well data are not available (Castagna et al., 1993).

Rock-property trends for sandstones and shales

Sandstones and shales show fundamental differences in mineral composition and structure. They exhibit a wide range of AI and V_P/V_S values, mostly due to differences in the amounts of compaction and cementation realized during burial (e.g., Ehrenberg and Nadeau, 2005). The effects of burial on the acoustic properties of sandstones and shales are described here, and an example is illustrated in summary plots of AI and V_P/V_S in the Judd Basin, which is located in the Atlantic Margin, West of Shetland (Figure 2).

Sedimentary rocks become faster and denser (exhibit higher AI) as porosity is reduced during burial (Figure 2a). Sands and shales are deposited with high initial porosities (approximately 40% for sand and 60% to 70% for shale). Porosity is lost rapidly during initial burial, especially in shales, where water is expelled and platy minerals realign perpendicular to maximum (burial) stress. Porosity retention through the burial process is much greater in sandstones (which form reservoirs) than mudstones (which form seals) due to differences in framework properties of the sediment. Sandstones tend to be more rigid (faster) but less dense than shales. These opposing trends can result in sandstones and shales showing similar AI values. Indeed, sandstones may show either higher or lower AI than adjacent shales (Figure 2a). It is important to emphasise that sandstones and shales have different density versus velocity relationships (Figure 3a), and for a given velocity, sandstones always have a lower density than shales. Global data sets of V_P and ρ were established by Gardner et al. (1974) and later modified by Castagna et al. (1993). The latter are used in the following generic forward models:

$$\text{Sandstone } \rho = -0.0115\ V_P^2 + 0.261\ V_P + 1.515 \quad (2)$$

$$\text{Shale } \rho = -0.0261\ V_P^2 + 0.373\ V_P + 1.458, \quad (3)$$

where ρ is density in g/cc, and V_P is P-wave velocity in km/s.

V_P/V_S decreases with depth, reflecting the process of compaction, which starts immediately beneath the seabed (Figure 2b). Shales typically have higher V_P/V_S for a given depth of burial than sandstones due to the contrasting mineral structure of the two lithologies. This observation is important. A contrast in AI at a shale-sand interface is commonly ambiguous for the determination of lithology (see Figure 2a). However, sandstones typically exhibit lower values of V_P/V_S than adjacent mudstones, and therefore are commonly a more reliable indicator of lithology. The relationship of V_P to V_S for brine-filled sediments is commonly described using the formulas established by Greenberg and Castagna (1992) (Figure 3b):

$$\text{Sandstone } V_S = 0.8042\ V_P - 0.8559 \quad (4)$$

$$\text{Shale } V_S = 0.77\ V_P - 0.8674, \quad (5)$$

where V_S is shear-wave velocity in km/s, and V_P is P-wave velocity in km/s.

V_S increases linearly with respect to V_P for both sandstones and shales, the relationship taking the form $y = mx + c$. The relationship is not unitary ($y = mx$). V_P/V_S is infinity at a V_P of approximately 1400 m/s (seawater) and reduces to a minimum of 1.5 at a V_P of 6000 m/s (pure quartz). Equations 4 and 5 are probably sufficient for estimating V_S in most quartz-rich sandstones, but locally, for example, where rocks show very low velocity (V_P is less than 2000 m/s), there may be a benefit in using modified coefficients (Vernik et al., 2002).

For a given V_P, the predicted V_S is lower for shales (equation 5) compared to sandstones (equation 4). Furthermore, for a given AI, the contrasting

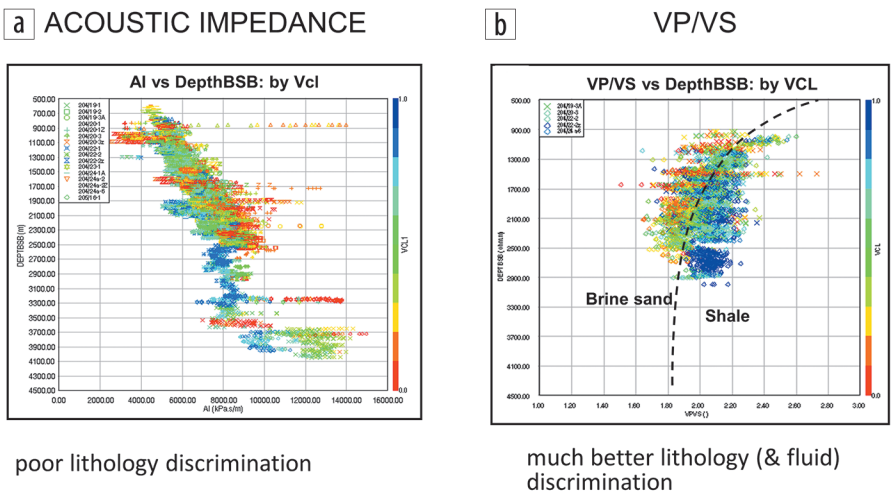

Figure 2. Burial depth trends for (a) AI and (b) V_P/V_S ratio for sedimentary rocks in Judd Basin, West of Shetland, Atlantic Margin. The Tertiary-age sedimentary rocks (to 2700 m below seabed) are normally pressured and typical of many frontier basins. After Went et al. (2005).

velocity-density relationships of sandstones and shales determine that shales exhibit lower V_P than sandstones (Figure 3a) (equations 2 and 3). These combined effects generally cause the V_P/V_S ratio to be lower in sandstones than an adjacent shale (Figure 2b).

Hydrocarbons have not been mentioned yet but clearly impact the velocity and density of porous sedimentary rocks. They have the effect of lowering ρ and V_P but cause a slight increase in S-wave velocity. As a result, the AI and V_P/V_S responses are lowered in the presence of hydrocarbon. The magnitude of the effect is determined mainly by the amount of porosity and the velocity and density of the hydrocarbon (Smith et al., 2003).

Rock properties and generic forward models of seismic reflectivity

The global empirical relationships of V_P, V_S, ρ, and lithology (described earlier) are used to model a range of outcomes of seismic reflectivity using the linearized two-term Shuey approximation (equation 1). The data used are presented in Table 1, and the modeled reflections are illustrated in Figures 4a–4c. The modeled data sit within the main field of data shown at 1750 m in Figure 2, and as such, may be considered representative of normally pressured strata at a depth of about 1750 m below the seabed. The only author-selected data values in Table 1 relate to V_P. Values for ρ and V_S are determined by equations 2–5 and are for brine sands only. Gassmann fluid substitution (Smith et al., 2003) is used to estimate the response of an equivalent hydrocarbon-filled section (light oil) (Figure 4c). The plots show the modeled reflections to 35° in a solid line. The lines are extrapolated to 90° ($\sin^2\theta = 1$) in order to identify the theoretical (extended) angles required for optimally identifying lithology and fluid.

Many reflections in seismic data result from shale-on-shale interfaces. A synthetic AVA model is shown in Figure 4a, where a hard inorganic shale (shale 2) underlies a softer inorganic shale (shale 1). This sets up an AI contrast so a positive reflection coefficient is returned at zero offset. The contrast in V_P/V_S between the two shales is small but slightly lower in shale 2, causing reflectivity to decrease with offset, reaching a projected reflection coefficient of zero at a $\sin^2\theta$ value of 0.54 (θ = 48°). Repeating this experiment with shale 2 on top yields a mirror image reflection. Adding further shales with harder or softer properties (not shown for clarity) yields further reflections. All show reflectivity

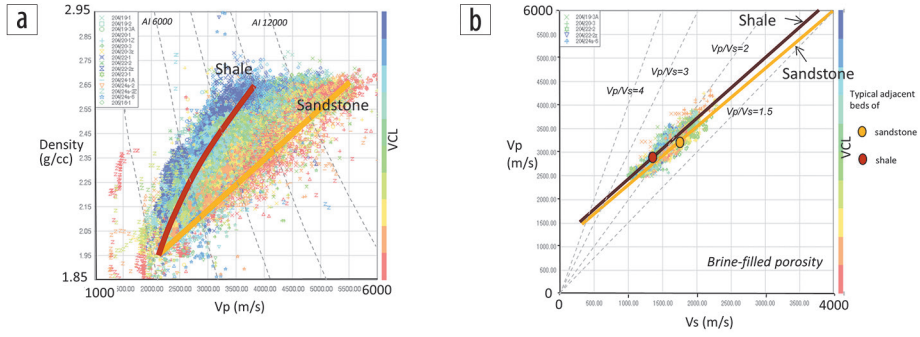

Figure 3. (a) Velocity versus density relationship for sandstones and shales in Judd Basin. For a given velocity, sandstones show a lower density than shales. (b) V_S versus V_P for sandstones and shales in Judd Basin, with the empirical estimators of Greenberg and Castagna (1992) overlain. For a given V_S, sandstones show a slightly lower V_P than shales. For a given impedance, sandstones show a higher V_P than shales and a lower V_P/V_S.

Table 1. Input data for sands and shales derived from global relationships of V_P to V_S and ρ used to create the models of angle-dependent reflectivity. For fluid substitution, the following in-situ fluid properties were used: oil density (0.7), bulk modulus (0.85), water density (0.98), and bulk modulus (2.57).

Input data	Shale 1	Shale 2	Org. Shale	Sand 1	Sand 2	Sand 3	Sand 4
V_P (m/s)	3048	3260	2700	3672	3300	3048	2800
V_S (m/s)	1480	1643	1420	2097	1798	1595	1396
Density (g/cc)	2.35	2.40	2.22	2.32	2.25	2.20	2.16
AI (m/s/g/cc)	7170	7813	5994	8513	7429	6717	6048
V_P/V_S	2.06	1.98	1.90	1.75	1.84	1.91	2.01
Porosity (%)				20%	24%	27%	30%

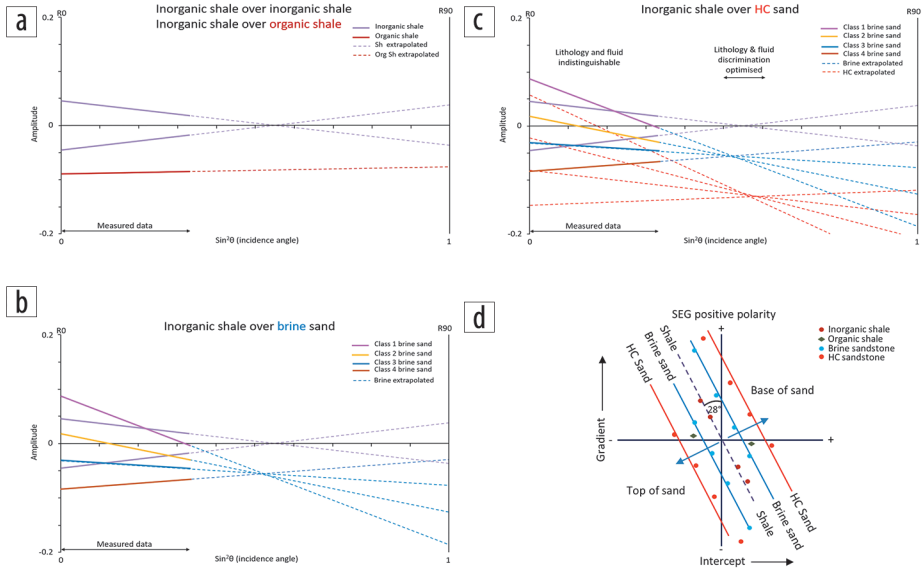

Figure 4. Models of angle-dependent reflectivity (linearized using $\sin^2\theta$) for sands and shales derived from global relationships of V_P, V_S, and ρ. (a) Shale over shale. (b) Shale over brine sand. (c) Shale over brine and oil sand. (d) The same data plotted on an intercept-gradient crossplot.

at zero offset but show the reflection coefficient decreasing with offset to reach a projected reflection coefficient of zero at approximately $\sin^2\theta = 0.54$ ($\theta = 48°$). This angle, which can be considered the minimum energy angle (Hicks and Francis, 2006), is the equivalent of the shale line in an intercept-gradient crossplot (Figure 4d).

Most shales are inorganic (or have very low total organic carbon). However, some shales are very rich in organic carbon and form hydrocarbon source rocks. These shales are soft relative to inorganic shales and do not share the same V_P/V_S relationships. They show low AI and low V_P/V_S, particularly when mature, due to high kerogen content (Loseth et al., 2011; Vernik et al., 2018). They are also prone to showing velocity anisotropy (Vernik and Liu, 1997). These rocks show a strong negative reflection coefficient at zero offset and tend to exhibit a near-zero to positive gradient (class 4) when overlain by an inorganic shale. Angle-dependent reflectivity can vary because velocity anisotropy materially impacts the AVA gradient (Rüger, 1997).

Figure 4b considers scenarios of inorganic shale (shale 1) capping brine-filled sandstone. Four sandstone types are considered, each with unique AI. The intercept-gradient relationships are all different, but when extrapolated to wider angles, they converge at a point that defines a negative reflection coefficient of approximately −0.06 at $\sin^2\theta = 0.53$ ($\theta = 47°$). This is similar to the angle at which shale-on-shale reflections are negligible. Changing the AI of the capping shale (not shown for clarity) changes the zero-offset reflection coefficient, but the point at which all extrapolated gradients converge is similar: −0.06 at $\sin^2\theta = 0.53$ ($\theta = 47°$). This point is the equivalent of the sand line in an intercept-gradient crossplot (Figure 4d).

Figure 4c takes the four sandstones in Figure 4b and uses fluid substitution to estimate angle-dependent reflectivity in the presence of light (gassy) oil using the Gassmann theory. The effect is to lower the intercept and alter the gradient. When extrapolated, the intercept-gradient combinations converge at a point that defines a strong negative reflection coefficient of approximately −0.125 at $\sin^2\theta = 0.55$ ($\theta = 48°$), closely comparable to the angle at which brine sands and shales converge. This is the hydrocarbon sand line in Figure 4d.

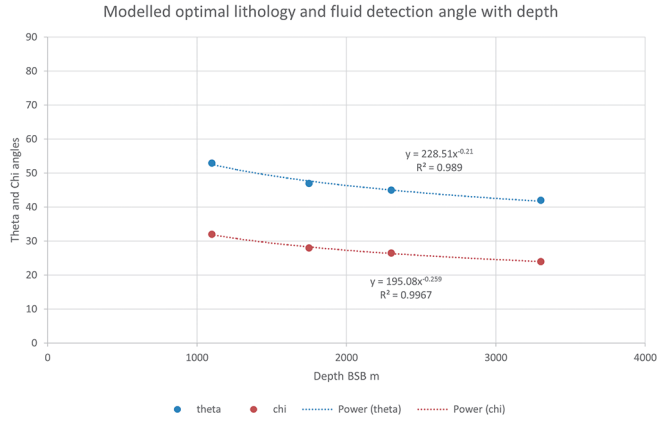

Figure 5. The relationship between the optimal lithology and fluid detection angle (θ and χ) and depth below seabed, as determined from global relationships of V_P, V_S, and ρ.

The intercept-gradient crossplot is commonly illustrated in publications dealing with AVA. The extended two-term reflectivity diagram, with multiple models displayed, enables the optimum incidence angle for lithology and fluid to be determined without resorting to intercept-gradient crossplots or alternative extended elastic impedance (EEI) methodologies. The notional or extended "reflectivity" at an incidence angle of 47° in this example usefully discriminates both lithology and fluid via the magnitude and polarity of the reflection coefficient (Figure 4d). The angle θ on this plot is related to the intercept-gradient crossplot angle χ by the formula $\sin^2\theta = \tan\chi$ (Whitcombe et al., 2002).

The experiment can be repeated for different depths of burial, e.g., 1100, 2300, and 3300 m. Comparable results are returned. However, the minimum energy and crossplot rotation angles shift progressively with depth. Shallower burial depths (1100 m) show zero shale-shale reflectivity at $\sin^2\theta = 0.63$ ($\theta = 53°$, $\chi = 33$), whereas deeper targets at 2300 and 3300 m show zero shale-shale reflectivity at $\sin^2\theta = 0.5$ ($\theta = 45°$, $\chi = 27$) and $\sin^2\theta = 0.44$ ($\theta = 42°$, $\chi = 24$), respectively (Figure 5). The gradual change in incidence angle (θ) or rotation angle (χ), required to resolve lithology and fluid effects, is driven by the propensity for the average V_P/V_S to decrease with depth (Castagna and Swan, 1997) (Figure 2b).

Application and discussion

Opinions vary on the best way to calibrate measured rock-property relationships to those derived from seismic inversion (e.g., Ball et al., 2014). It is my preference to avoid direct use of wells in the process and use relative impedance inversion to limit the impact of noise in gradient and trace math calculations (Cambois, 2000). By comparing standalone seismic inversion results with well-based observations, a judgement can easily be made as to the viability of using AVA in a seismic data set for lithology and fluid detection. Using this approach, it is my experience (based largely on data from the eastern Atlantic Margin, Norway, to southern Africa) that the match to forward models is robust, at least when working with modern 3D seismic data sets (e.g., Went et al., 2005). The incidence angle θ at which lithology and fluid are optimally discriminated in the generic forward models presented earlier is not particularly wide (approximately 45° for most likely target depths). Therefore, it is a relatively simple exercise to generate an extrapolated reflectivity or EEI attribute using either near- and far-angle stacks or intercept-gradient information from prestack gathers (Figure 6a). The EEI θ angle of 45° should not be confused with the data acquisition angle, which cannot be used as a surrogate.

An example seismic attribute, relative extended elastic impedance (rEEI) at $\theta = 45°$, is presented in Figure 6d. It is shown alongside seismic stack reflectivity and relative AI (Figures 6b and 6c). The stack shows many reflections that rEEI(θ)45 does not have. Many may be deduced as shale-on-shale reflections, which the forward model suggests should disappear at 45°. Hence, the attribute shows significant background red color, indicating lithology of a similar neutral impedance. A low extended elastic impedance anomaly is detected at 4 s two-way time on the rEEI(θ)45 attribute and is manifested as an anomalous intercept-gradient relationship on the AVA crossplot

(Figure 6e). The anomaly is identified as a candidate hydrocarbon-bearing sand in a pinch-out trap formed at the basin margin.

Time-windowed crossplots of seismic reflection AVA data are not without problems. It has long been recognized that a noise trend cuts through seismic reflection data in intercept-gradient space. Correlated noise (Cambois, 1998) typically results in a background trend in intercept-gradient crossplots that is steeper than that of the rock-property trend. The angle represented by this correlated noise on the crossplot varies according to the data set, incident angle range, and therefore depth, but is typically in the range of 12°–20° (Hendrickson, 1999). How detrimental to AVA analysis it is depends to a large extent on the assumed angle of the background rock-property trend on an intercept-gradient crossplot. It is sometimes assumed that background V_P/V_S is 2, in which case the background rock-property ellipse lies at an angle of 45° on an intercept-gradient crossplot (Simm et al., 2000). In this case, the noise trend cuts across the rock-property trend at a high angle, potentially obscuring all but some class 3 and 4 anomalies. The modeling in this study, however, indicates that the typical background rock-property trend is 22°–28°, which is reasonably close to the correlated noise trend. As a result, the noise trend intersects the background data trend with significance only at the extreme ends of the background data ellipse. Most anomalies reside outside of the noise envelope and remain detectable. Practical experience suggests that hydrocarbon anomalies relating to class 2P, 2, 3, and 4 can be detected in time-windowed crossplots or an equivalent angle attribute. Class 1 anomalies may remain a problem where substitution of hydrocarbons for brine lowers the intercept and moves the data point into, rather than away from, the noise envelope component of the background trend.

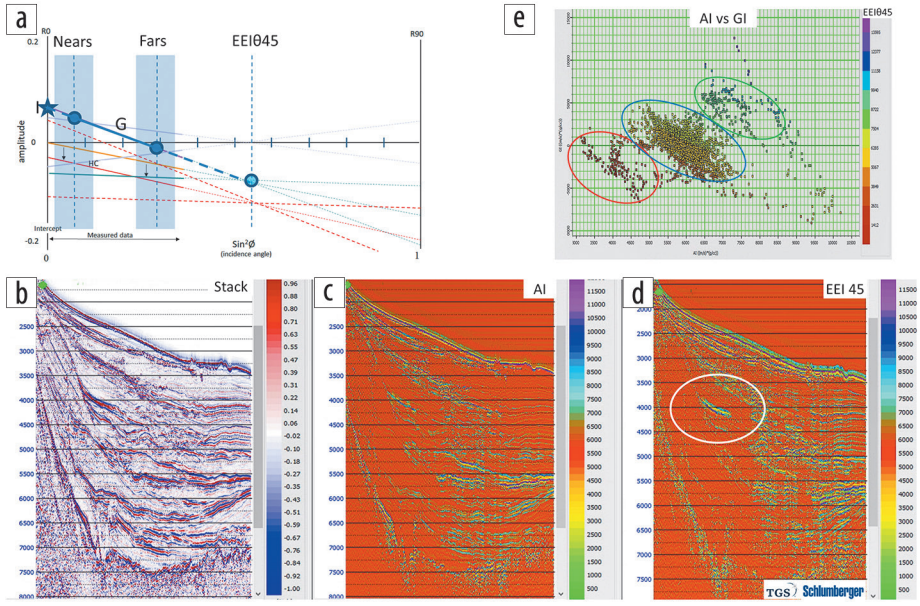

Figure 6. Inversion routine and example result from offshore Mozambique. (a) Inversion routine generating relative AI and EEI(θ)45 from the near- and far-angle stacks. (b) Full stack. (c) Relative AI. (d) Relative EEI(θ)45 highlighting anomaly (circled). (e) AI versus GI crossplot showing the anomaly (circled in red). Note that the color coding of the crossplot is EEI(θ)45, confirming that the attribute EEI(θ)45 is a representation of the AI versus GI crossplot. Data courtesy of TGS and Schlumberger.

Conclusions

Global relationships between V_P, V_S, and ρ are used to build generic two-term forward models of AVA for siliciclastic basins. These models predict that lithology and fluid can be discriminated using extended elastic impedance, or reflectivity, at an incidence angle of about 45° (θ) for most depths of interest when exploring frontier basins with simple burial histories. This equates to an intercept-gradient crossplot angle of 26.5°. An example is presented where the attribute rEEI(θ)45 highlights a candidate fluid anomaly in a sandstone pinch-out trap formed at the basin margin in offshore Mozambique. A correlated noise trend in seismic reflection data crossplots of intercept and gradient typically lies at an angle of approximately 15° and is commonly cited as a factor that limits the power of AVA to resolve hydrocarbon anomalies in time-windowed crossplots or equivalent weighted stacks. This study suggests that the main noise trend lies close enough to the background rock-property trend to prevent it from obscuring anomalies in most cases in intercept-gradient space. TLE

Acknowledgments

Grateful thanks are extended to Mike Owens for providing helpful comments and feedback on the manuscript prior to submission, an anonymous reviewer for constructive criticism that helped significantly improve the final draft, and TGS for permission to publish.

Data and materials availability

Data associated with this research are available and can be obtained by contacting the corresponding author.

Corresponding author: david.went@tgs.com

References

Avseth, P., T. Mukerji, and G. Mavko, 2005, Quantitative seismic interpretation: Cambridge University Press.

Ball, V., L. Tenorio, J. P. Blangy, M. Thomas, and C. Schiott, 2014, Uncertainty quantification of two-term relative elastic inversion: Presented at the 2nd Integrated Reservoir Modelling Conference, EAGE, https://doi.org/10.3997/2214-4609.20147465.

Cambois, G., 1998, AVO attributes and noise: Pitfalls of crossplotting: 68th Annual International Meeting, SEG, Expanded Abstracts, 244–247, https://doi.org/10.1190/1.1820390.

Cambois, G., 2000, AVO inversion and elastic impedance: 70th Annual International Meeting, SEG, Expanded Abstracts, 142–145, https://doi.org/10.1190/1.1815671.

Castagna, J. P., and H. W. Swan, 1997, Principles of AVA crossplotting: The Leading Edge, **16**, no. 4, 337–344, https://doi.org/10.1190/1.1437626.

Castagna, J. P., M. L. Batzle, and T. K. Kan, 1993, Rock physics: The link between rock properties and AVO response, *in* J. P. Castagna and M. M. Backus, eds., Offset-dependent reflectivity — Theory and practice of AVO analysis: SEG Investigations in Geophysics, **8**, 135–171.

Ehrenberg, S. N., and P. H. Nadeau, 2005, Sandstone vs. carbonate petroleum reservoirs: A global perspective on porosity-depth and porosity-permeability relationships: AAPG Bulletin, **89**, no. 4, 435–445, https://doi.org/10.1306/11230404071.

Gardner, G. H. F., L. W. Gardner, and A. R. Gregory, 1974, Formation velocity and density — The diagnostic basics for stratigraphic traps: Geophysics, **39**, no. 6, 770–780, https://doi.org/10.1190/1.1440465.

Greenberg, M. L., and J. P. Castagna, 1992, Shear-wave velocity estimation in porous rocks: Theoretical formulation, preliminary verification and applications: Geophysical Prospecting, **40**, no. 2, 195–209, https://doi.org/10.1111/j.1365-2478.1992.tb00371.x.

Hendrickson, J. S., 1999, Stacked: Geophysical Prospecting, **47**, no. 5, 663–705, https://doi.org/10.1046/j.1365-2478.1999.00150.x.

Hicks, G. J., and A. M. Francis, 2006, Extended elastic impedance and its relation to AVO crossplotting and V_P/V_S: 68th Conference and Exhibition, EAGE, Extended Abstracts, https://doi.org/10.3997/2214-4609.201402386.

Løseth, H., L. Wensaas, M. Gading, K. Duffaut, and M. Springer, 2011, Can hydrocarbon source rocks be identified on seismic data?: Geology, **39**, no. 12, 1167–1170, https://doi.org/10.1130/G32328.1.

Rüger, A., 1997, P-wave reflection coefficients for transversely isotropic models with vertical and horizontal axis of symmetry: Geophysics, **62**, no. 3, 713–722, https://doi.org/10.1190/1.1444181.

Shuey, R. T., 1985, A simplification of the Zoeppritz equations: Geophysics, **50**, no. 4, 609–614, https://doi.org/10.1190/1.1441936.

Simm, R., R. White, and R. Uden, 2000, The anatomy of AVO crossplots: The Leading Edge, **19**, no. 2, 150–155, https://doi.org/10.1190/1.1438557.

Smith, T. M., C. H. Sondergeld, and C. S. Rai, 2003, Gassmann fluid substitution: A tutorial: Geophysics, **68**, no. 2, 430–440, https://doi.org/10.1190/1.1567211.

Vernik, L., and X. Liu, 1997, Velocity anisotropy in shales: A petrophysical study: Geophysics, **62**, no. 2, 521–532, https://doi.org/10.1190/1.1444162.

Vernik, L., D. Fisher, and S. Bahret, 2002, Estimation of net-to-gross from P and S impedance in deepwater turbidites: The Leading Edge, **21**, no. 4, 380–387, https://doi.org/10.1190/1.1471602.

Vernik, L., J. Castagna, and S. J. Omovie, 2018, S-wave velocity prediction in unconventional shale reservoirs: Geophysics, **83**, no. 1, MR35–MR45, https://doi.org/10.1190/geo2017-0349.1.

Went, D., G. Roberts, and R. Morgan, 2005, Fluid and lithology discrimination using angle-specific facies finder: An example from the Blane Field area, Paleocene, CNS: Force Presentation, NPD.

Whitcombe, D. N., P. A. Connolly, R. L. Reagan, and T. C. Redshaw, 2002, Extended elastic impedance for fluid and lithology prediction: Geophysics, **67**, no. 1, 63–67, https://doi.org/10.1190/1.1451337.